Dynamic and static properties of the concentrated micellar solution and gel phase of a triblock copolymer in water

Helmut Lindner, Günther Scherf, and Otto Glatter*
Institut für Chemie, Karl-Franzens-Universität, Graz, Austria
(Received 10 July 2002; revised manuscript received 23 December 2002; published 16 June 2003)

The dynamic and static behavior of the poly(ethylene oxide)-poly(propylene oxide)-poly(ethylene oxide) triblock copolymer ''P94'' is studied in aqueous solution. This polymer forms transparent micellar phase structures through the whole phase diagram. The characteristics of these structures can be tuned by variation of temperature and concentration. The transparent gel at high concentrations and at ambient temperatures is the main interest in this study. The transition from the ergodic solution to this nonergodic gel or glass state can be reached in two ways: at constant temperature with an increase of concentration or at constant concentration with increasing temperature. We characterize the system in both ways with dynamic and static light scattering and with small-angle x-ray scattering experiments. At 40 °C, no concentration dependent change in the micellar structure of the system can be detected from the small-angle x-ray scattering results. Even in the gel we find globular particles. This is important for the evaluation and interpretation of the dynamic light scattering measurements. In the ergodic phase region at constant temperature, we find that a ratio of 2.17 gives a perfect fit to the experimental data when we allow the effective volume fraction to be proportional to the mass fraction. In the gel region we find two diffusional decays in the intensity correlation functions and an arrested part. The diffusion coefficients from the faster decay stay constant inside the gel and the nonergodicity parameter increases linearly with concentration. Both, the fast and slow diffusional modes show no angular dependence of their scattering intensities, indicating their origin from small objects, while the arrested mode comes, as expected, from structures larger than the resolution of the experiments.

DOI: 10.1103/PhysRevE.67.061402 PACS number(s): 82.70.Uv, 82.70.Gg

I. INTRODUCTION

Triblock copolymers of type polyethylene oxide (PEO)-polypropylene oxide-polyethylene oxide are nonionic surfactants and are of great interest for many applications and as a model system for basic research. The behavior of aqueous solutions of this type of molecules is well known due to the large number of publications concerning the aggregation, gelation and micellization [1–4], the phase behavior [5–7], and the influence of the relative block size [8,9]. The substance of interest in this contribution is P94, a polymer with a mean number of 21 ethylene oxide units in the outer blocks and a mean number of 47 propylene oxide units in the inner block, resulting in a molecular weight of 4700 g/mol and a weight fraction of about 40% for the two ethylene oxide chains. This polymer forms globular micelles at low concentrations and a stiff and transparent gel at high concentrations at ambient temperatures. The main interest in this study is the transition from the fluid, ergodic into the arrested nonergodic state and concerns the dynamic and static properties in the stiff gel region. We characterize this system with dynamic and static light scattering (SLS) and with small-angle x-ray scattering.

First we give a short review of the dynamic and static behavior in the ergodic phase region. The main part of this contribution describes the nonergodic gel region, which can be reached in two ways: at constant temperature with an increase of concentration or at constant concentration with increasing temperature. In this second scan we increase the effective concentration of micelles at fixed total concentration of polymer, as more and more unimers self-assemble into micelles with increasing temperature. Each of the two possible transitions has been investigated.

II. THEORETICAL BACKGROUND

A. Dynamic light scattering in ergodic media

From the time-dependent ensemble averaged intensity fluctuations, measured at a fixed angle, the ensemble averaged intensity autocorrelation function $\langle \mathrm{ICF} \rangle_E$, $g_E^{(2)}(\boldsymbol{q},t)$ is calculated. In the case of an ideal homodyne experiment (Gaussian beam), this $\langle \mathrm{ICF} \rangle_E$ corresponds to the ensemble averaged field correlation function $\langle \mathrm{FCF} \rangle_E$, $g_E^{(1)}(\boldsymbol{q},t)$ with

$$g_E^{(2)}(\boldsymbol{q},t) = A[1+\beta^2(g_E^{(1)2}(\boldsymbol{q},t))] = A\left[1+\beta^2\left(\sum_i N_i \alpha_i^2 P_i e^{-q^2 D_i t}\right)^2\right], \quad (1)$$

where $\boldsymbol{q}$ is the scattering vector and q is its magnitude. N_i is the number concentration of the ith component and t, α_i, P_i, D_i are time, polarizability, form factor, and the diffusion coefficient, respectively. A is the mean squared intensity and β^2 is the coherence factor. For diluted solutions, the diffusion coefficient D can be related to the hydrodynamic radius R_H by the Stokes-Einstein equation

$$D = \frac{kT}{6\pi\eta R_H}, \quad (2)$$

*Author to whom correspondence should be addressed.

where k, T, and η are the Boltzmann constant, the absolute temperature, and the viscosity, respectively.

For polydisperse systems it is convenient to define a continuous size distribution function IDF. Let $F(R)dR$ be the fraction of particles with radius R between R and $R+dR$. P_i, D_i, and α_i are also functions of R. For a continuous distribution of particles, the sum in Eq. (1) can be replaced by an integral

$$\frac{g_E^{(2)}(\boldsymbol{q},t)}{A}-1=\beta^2\left(\int_0^\infty \alpha^2(R)F(R)P(R)e^{-q^2D(R)t}dR\right)^2. \tag{3}$$

The IDF's, calculated by inverse Laplace transformation, show the weights of all classes of particles that contribute to the intensity signal [10].

B. Dynamic light scattering in nonergodic media

In nonergodic media the diffusional motion of the particles is hindered. The duration of standard dynamic light scattering (DLS) measurement, with data acquisition times from minutes to several hours, is not long enough that the particles can take all possible configurations one to each other (ensemble average). In the extreme case of a frozen structure, even an infinite measuring time would not lead to the ensemble average. Therefore, the result of one measurement can only be a time average of the intensity correlation function $\langle \mathrm{ICF}\rangle_T$. The theory of the dynamic properties of nonergodic media is already worked out in great detail [11]. The calculation of $\langle \mathrm{FCF}\rangle_E$ from $\langle \mathrm{ICF}\rangle_T$ from a single correlation measurement is the main information in that paper for our need. The corresponding equation reads

$$g_E^{(1)}(\boldsymbol{q},t)=1+\frac{\langle I(\boldsymbol{q})\rangle_T}{\langle I(\boldsymbol{q})\rangle_E}\left[\sqrt{\frac{g_T^{(2)}(\boldsymbol{q},t)-g_T^{(2)}(\boldsymbol{q},0)+1}{\beta^2}}-1\right], \tag{4}$$

where $\langle I(\boldsymbol{q})\rangle_T$ and $\langle I(\boldsymbol{q})\rangle_E$ are the time and the ensemble averaged mean intensities and β^2 is the coherence factor. $\langle I(\boldsymbol{q})\rangle_E$ and β^2 have to be determined by additional measurements. To obtain the ensemble averaged mean intensity, the sample is rotated in the incident beam during the detection of the intensity to assure all possible configurations to be achieved. The coherence factor is taken from measurements of a diluted, monodisperse latex dispersion in water (ideal ergodic sample). This factor is also a measure for the quality of the experimental setup. The knowledge of $\langle \mathrm{FCF}\rangle_E$ allows one to use all evaluation routines used in standard DLS experiments as described in Sec. II A. With this procedure, the correct size or size distribution can be determined.

C. Small-angle x-ray scattering

The technique of small-angle x-ray scattering (SAXS) is a powerful tool for determining the size, shape, and internal structure of particles in the size range from a few nanometers to about 100 nm [12]. One detects the angle-dependent intensity of the scattered x-rays, where q is the length of the scattering vector $\boldsymbol{q}$ and is related to the scattering angle Θ by

$$q=|\boldsymbol{q}|=\frac{4\pi}{\lambda}\sin\frac{\Theta}{2}, \tag{5}$$

where λ is the wavelength. The measured intensity is given by

$$I(q)=4\pi\int_0^\infty p(r)\frac{\sin(qr)}{qr}dr, \tag{6}$$

where $p(r)$ is the pair distance distribution function of the particles. For the determination of the size and shape of a particle, it is easier to interpret the $p(r)$ function in real space compared to the $I(q)$ in reciprocal space. The total scattering intensity can be expressed in the following factorization:

$$I(q)=nP(q)S(q), \tag{7}$$

where n is the particle density. This factorization is strictly valid only for monodisperse spherical symmetric interacting particles and for noninteracting asymmetric objects. A similar description is possible for polydisperse systems, where the scattering curve can be related to the product of the form factor of particles $\overline{P}_{ave}(q)$ times the effective or ''measured'' structure factor $S_{eff}(q)$ [13]. Fourier transformation of the form factor $P(q)$ results in the $p(r)$ function [14]. This calculation is facilitated completely model-free with minimized termination effects and requires only a rough estimation of the maximum dimension of the particles when using the indirect Fourier transformation (IFT) method [15,16]. The generalized transformation method GIFT [14,17] allows simultaneous calculation of $P(q)$ and $S(q)$, where only $S(q)$ is model dependent. For the uncharged system under investigation, we assume a hard sphere interaction potential and use the Percus-Yevick approximation as closure relation. The idea of the GIFT method is that the Fourier transformed real space base functions are multiplied with a parametrized $S(q)$ prior to fitting to the measured scattering curve in reciprocal space. This makes the problem highly nonlinear and, therefore, the method is based on the Boltzmann simplex simulated annealing algorithm to find the global minimum [17]. The form factor is completely model-free in these calculations, i.e., there are no assumptions about shape and inner structure made. The only *a priori* information used for $P(q)$ is an upper estimate of the maximum dimension of the particles.

III. EXPERIMENTAL SECTION

The light transmission measurements were performed with the sample in a cylindrical cuvette (inner diameter 8 mm) fixed in a temperature controlled cuvette holder. A He-Ne laser (10 mW) was used as light source and a photodiode as detector. The measurements were done by detecting the electric current of the diode illuminated by the transmitted beam after 15 min of temperature equilibration.

A laboratory built goniometer equipped with an Ar^+ laser (514.5 nm, BeamLok 2060-5S, Spectra Physics, Darmstadt, Germany) was used for the dynamic light scattering measurements. The detection optics consisted of a single mode

fiber (OZ from GMP, Zürich, Switzerland) coupled to an ALV/SO-SIPD/DUAL photomultiplier with pseudo-cross-correlation setup, ALV-5000 multiple tau digital correlator with ALV-5000/FAST extension (all from ALV, Langen, Germany). All experiments were performed using two polarizers (Glan Thomson prisms, Halle, Berlin, Germany, discrimination $<10^{-6}$) both in vertical orientation, one in front of the sample cell, the other between the sample and the entrance of the single mode fiber. As data acquisition software the ALV-5000/E program was used.

The data acquisition at each point in the ergodic region of the phase diagram was typically done by measuring the intensity correlation functions with an effective laser power of 200 mW after a time of two h for temperature equilibration. The duration for the detection of one curve was chosen to be 100 s. The averaged functions (four to six curves), which had a total sum of at least 10^7 counts, were fitted by the method of cumulants [18] and evaluated by inverse Laplace transformation [10].

In the nonergodic region, the time averaged intensity correlation functions were measured in the following way. From each sample, five curves, of 1000 s each, were detected after overnight temperature equilibration. Then the position of the sample was changed to produce another speckle, and the measurement was repeated. This procedure was done four to five times and the results were stored without averaging. The ensemble averaged intensity was obtained by rotating the sample during intensity detection. From ten measurements, of 30 s each, the ensemble averaged intensity was finally calculated.

For the SAXS measurements, we used a rotating-anode generator (AXS, Bruker, Karlsruhe, Germany) with a Cu target operated at 40 kV and 100 mA. The divergent x-ray beam from the anode was cleaned from hard x-rays and the Cu K_β line and was collimated by a so called Göbel mirror (AXS Bruker, Karlsruhe, Germany). A modified Kratky compact camera was used as a block collimation system. The intensity was detected by an imaging-plate detector (Fuji BAS 1800) with AIDA software (Raytest, Straubenhardt, Germany) [12].

P94 from ICI (Imperial Chemical Industries, UK) was used for the experiments as received without further purification. The solutions were made weighting the polymer and water, obtained from a Milli-Q RG (Millipore, Ireland), to give the used concentrations in mass fractions $[\%(w/w)]$.

The viscosity measurements have been performed using a prototype of the DMA 5000, which has been modified by the addition of an ultrasonic sound cell equivalent to DSA 48 (both Anton Paar KG, Graz, Austria). This density meter works on the basis of an oscillating tube. The damping of the oscillating tube can be converted into actual viscosity data up to about 300 mPa s [19]. The viscosities measured with this instrument result from ultralow shear stress. A temperature equilibration time of 15 min was given to the samples prior to the measurements.

IV. RESULTS

A. Phase diagram

The phase diagram of the system is shown in Fig. 1. The phase boundaries were detected using ultrasonic speed, viscosimetry, and light transmission measurements. The structure of the single phases was determined with SAXS, small angle neutron scattering and depolarized DLS (unpublished results). At low concentrations and temperatures unimers of the polymer exist in solution with a small amount of large aggregates. Increasing the temperature yields a phase of coexisting unimers and spherical micelles; the lowest full line indicates the formation of the first micelles; at the second full line the formation of micelles is completed. The dashed line in between is the region with maximum formation rate of the micelles. At higher temperatures, a phase consisting of nearly monodisperse spherical micelles exists. Further increase in temperature leads to a shape change from spherical micelles to cylindrical micelles [20].

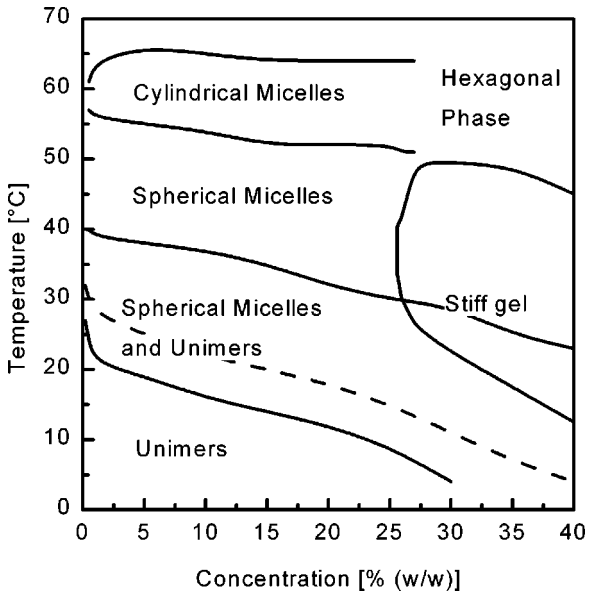

FIG. 1. The phase diagram of the triblock copolymer P94 in aqueous solution as a function of temperature and concentration.

At high concentrations, we already start at low temperature with a mixture of unimers and micelles. Increasing the temperature, a sharp phase boundary to a stiff gel region is found. In this region a transparent and nonergodic system is formed. At even higher temperatures one finds a hexagonal phase formed by the cylindrical micelles.

In Fig. 2 we show some of the light transmission results in the concentration and temperature regime of the stiff gel. The gel boundary is visible by the drop in the transmission, indicating light scattering from narrow two-phase regions. The scattering intensity shows an enormous increase at the phase boundary. Since the measurements have been performed in a scan trough mode (only 15 min temperature equilibration at each step of 0.1 °C), it can not be expected that the samples have already reached thermodynamic equilibrium. Such an equilibration may take up to several days.

B. Concentration variation at constant temperature

SAXS experiments. For a correct interpretation of our DLS results, the knowledge of the shape of the particles is important. In Fig. 3 we show some of the SAXS curves measured

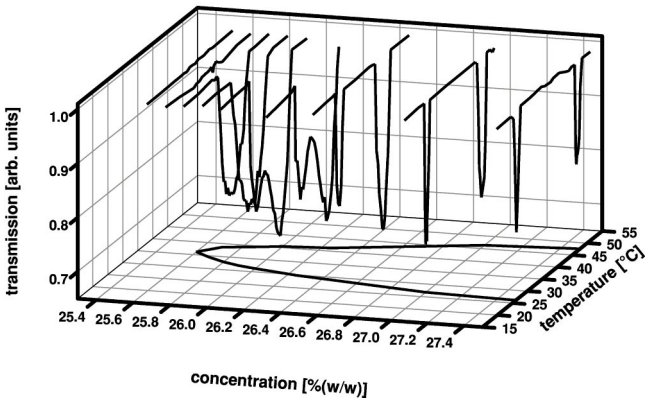

FIG. 2. Light transmission plotted vs concentration and temperature for a rough estimation of the phase boundary toward the stiff gel.

at 40 °C in different concentrations between 1 and 20% (w/w). From the typical side maxima it can be seen that the particles in the samples are rather spherical and monodisperse objects. At low q we see also the influence of particle interaction for the concentrated samples. The scattering intensity first increases due to the increase of concentration. Then, with further increase of concentration the intensity decreases because of the decreasing isothermal compressibility of the solution. When the curves are evaluated with the GIFT method and normalized to the concentration, we obtain in all cases approximately the same $p(r)$ functions, indicating globular and quite monodisperse particles with a diameter of about 15.5 nm (data not shown, similar to Fig. 4 in Ref. [5]). The increasing particle interactions at higher concentrations can be fitted within the statistical accuracy by hard sphere structure factors of nearly monodisperse spheres. The structure of the particles represented by its form factors does not change significantly in the concentration range measured, i.e., the micelles remain globular and there is no indication of existence of any larger

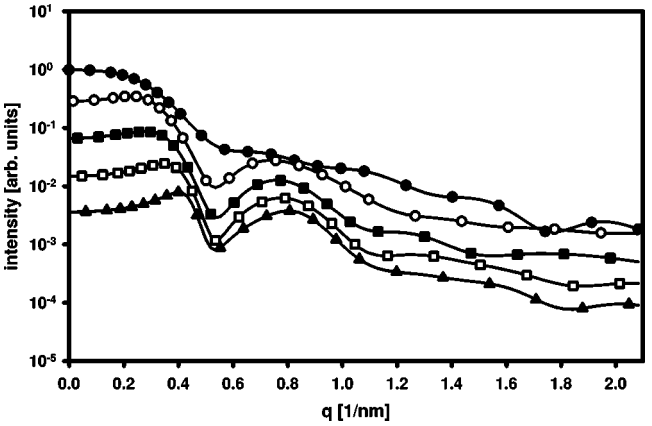

FIG. 3. The small-angle x-ray scattering curves of P94 are shown for different concentrations at 40 °C. The intensity is plotted in logarithmic scale vs scattering vector. The curves are scaled in height by arbitrary factors for better visibility and correspond to the following concentrations: ● 1, ○ 5, ■ 10, □ 15, and ▲ 20% (w/w).

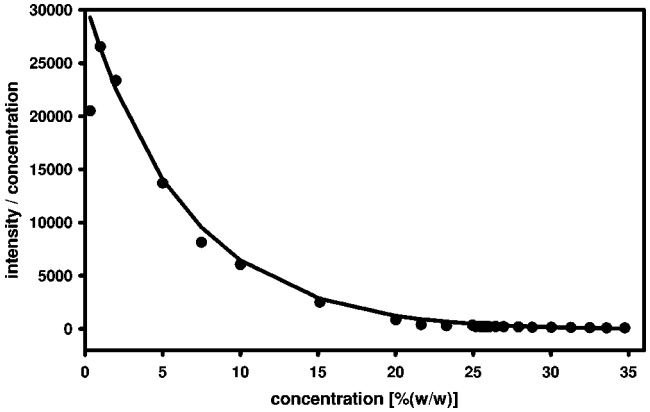

FIG. 4. The ensemble averaged scattering intensity divided by the concentration [c is the concentration in % (w/w)] compared with a theoretical structure factor $S_0(\Phi)$ is plotted vs concentration. The best fit for $S_0(\Phi)$ is obtained with $\Phi = 2.20c$.

aggregates in the micellar phase. Also the structure factor parameters are nearly constant and result in a hard sphere interaction radius R_{HS} of about 7.4 nm with a low polydispersity of a few percent only, and an effective volume fraction of interaction, which is about 2.1 times the concentration ($\Phi_{eff} = 2.1c/100$).

SLS experiments. This agreement with hard sphere interaction can also be found in a comparison of the static light scattering results with the theoretical structure factor $S_0(\Phi)$ for hard spheres [21]:

$$S_0(\Phi) = \frac{(\Phi - 1)^4}{(2\Phi + 1)^2} \tag{8}$$

when plotted versus the concentration (Fig. 4). The data points were calculated by dividing the ensemble averaged intensity by the concentration. The fit line is $S_0(\Phi)$ scaled by an arbitrary amplitude factor. The best fit is obtained by calculating Φ from 2.20 times the concentration in $[\%(w/w)]$.

DLS experiments. The diffusion coefficients, determined by dynamic light scattering at 40 °C as a function of concentration in the ergodic phase region are shown in Fig. 5. The result is compared with the hard sphere interaction approximation (dashed line)

$$D_{eff} = D_0(1 + 1.56\Phi), \tag{9}$$

where D_0 is determined to be 4.35×10^{-11} m^2/s, this corresponds to $R_H = 8.8$ nm. The slope does not match when the volume fraction Φ is set equal to the mass fraction (concentration $[\%(w/w)]$). Allowing the effective volume fraction to be proportional to the mass fraction, we find that a scaling factor of 2.17 gives a perfect fit to the data (full line).

Viscosimetry. Approaching the nonergodic region, the macroscopic viscosity is dramatically increasing as can be seen in Fig. 6. The fit curve is calculated according to Mooney [22],

$$\frac{\eta_S}{\eta_0} = \exp\left(\frac{2.5\Phi}{1 - K\Phi}\right), \tag{10}$$

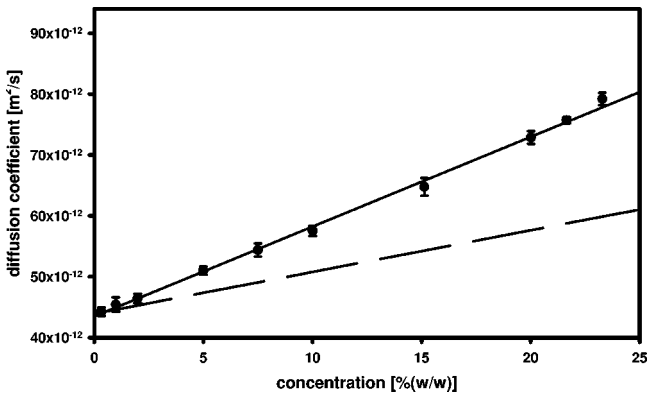

FIG. 5. The diffusion coefficients of P94 at 40 °C are plotted vs concentration. The dashed line describes a fit on the basis of hard sphere interaction using the mass fraction as the volume fraction. The full line is a fit with an effective volume fraction being proportional to the mass fraction with an optimized proportionality factor of 2.17.

where K denotes the self-crowding factor. η_S and η_0 are the viscosities of the solution and the solvent, respectively. Φ is the volume fraction of the dissolved particles. According to other results, Φ has been taken to be 2.1 times the concentration [% (w/w)]. The self-crowding factor has been determined to be 1.42, which lies on the lower side between the theoretical limits for monodisperse spheres of 1.35 and 1.91 and which is nearly identical to the value of 1.43 found by Mooney for viscosity data from suspended glass spheres [22]. The highest concentration was not used for the calculation of the fit.

C. DLS measurements in the nonergodic region

1. Fast and slow diffusion modes

First we show some angle dependent field correlation functions for a 35% (w/w) solution at 25 °C, in the center of the stiff gel, in Fig. 7. We see a fast and a slow decay and an arrested part at long times. From the q dependence of the

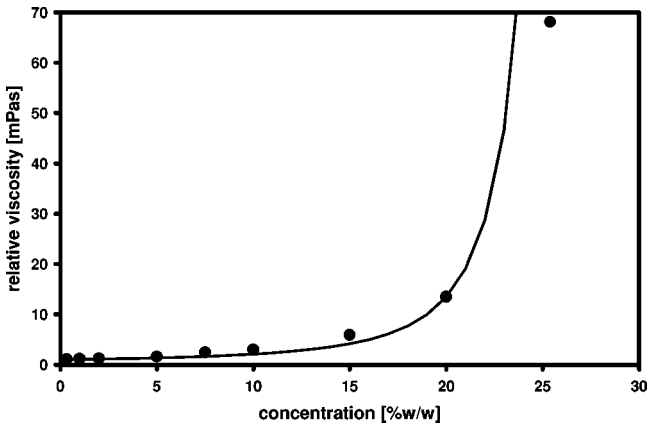

FIG. 6. The macroscopic relative viscosity, measured at 40 °C with the low shear instrument, is plotted vs concentration. The full line is a viscosity fit with fixed $\Phi = 2.10c$ according to the equation of Mooney. From the fit calculation, K was determined to give 1.42.

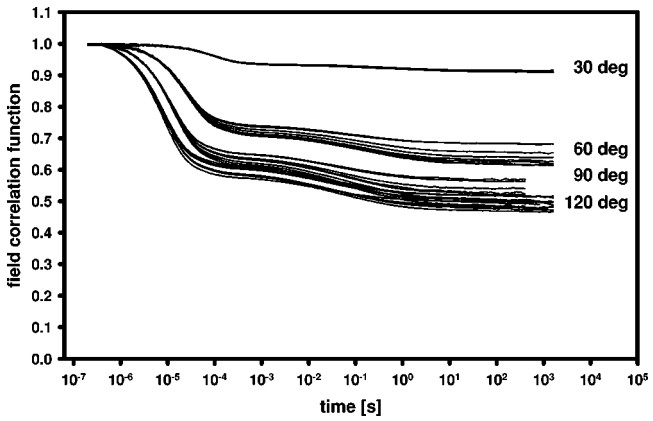

FIG. 7. Four bundles of field correlation functions corresponding to angles of 30°, 60°, 90°, and 120° are plotted vs time. The concentration of the sample was 35% (w/w) and temperature 25 °C.

correlation time, shown in Fig. 8, it can be concluded that both decays are diffusional terms as the slopes of both, the fast mode k_f, and of the slow mode k_s, agree with the theoretically predicted value of 2 within the statistical errors. Another possibility to check the diffusive behavior is by plotting the decay rates versus q^2. The result is two straight lines with zero intercept (not shown). It is also interesting to check the ratio of the amplitudes of the fast and slow modes as a function of the scattering angle. This ratio is calculated for each individual correlation function in the bundle measured for every scattering vector. The mean values show no significant angular dependence. A weighted mean over all angles yields a value of 3.6 for the ratio. The overall angular dependence is same for both modes.

From the field correlation function and the ensemble averaged mean scattering intensity, it is possible to calculate the portion of the intensity of each population that contributes to the signal [23]. The angle dependent intensities of the fast and slow diffusional modes and of the frozen state can be seen in Fig. 9. We see constant intensities for the fast and slow diffusional modes, whereas the intensity of the frozen

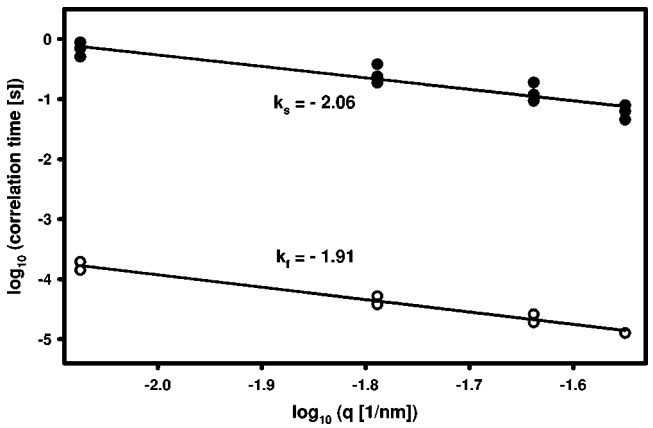

FIG. 8. The angular dependence of the correlation time of the fast (○) and the slow (●) decay from Fig. 7 in a double-$\log_{10}$ plot. A slope of 2 is predicted for diffusional motion.

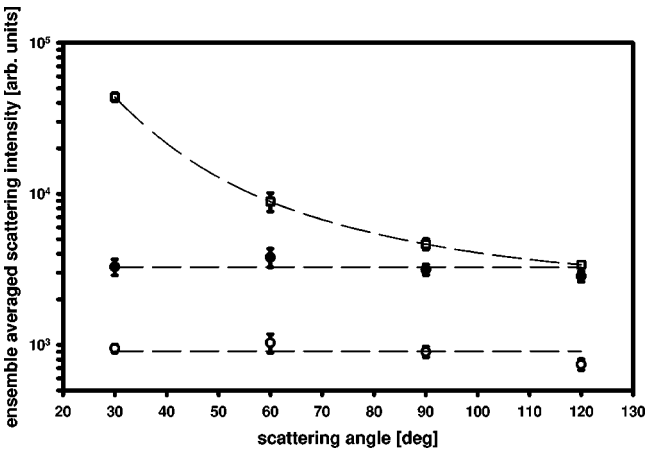

FIG. 9. The ensemble averaged mean scattering intensities from Fig. 7 of the fast (●) and slow (○) diffusional modes and of the frozen state (□) are plotted as a function of scattering angle.

state is dramatically increasing towards low angle. This indicates that the fast and the slow modes stem from small objects, while the frozen state originates from much larger structures.

2. Concentration dependence

In Fig. 10 we show the diffusion coefficients of the fast relaxation mode close to and inside the gel phase at a fixed temperature of 40 °C. The effective diffusion coefficient of the micelles increases linearly in the ergodic, fluid regime as also shown in Fig. 5 and turns into a practically constant fast mode inside the gel. This and the above findings allow us to conclude that the fast mode is the collective diffusion of the micelles in the gel.

The nonergodicity parameters $g_E^{(1)}(\boldsymbol{q},\infty)$ are shown in Fig. 11 as a function of concentration at 40 °C. Beyond 27% (w/w), the contribution of the arrested parts in the sample increases linearly with concentration.

3. Temperature dependence

The field correlation functions from a 35%(w/w) solution for different temperatures (Fig. 12) show only one decay at

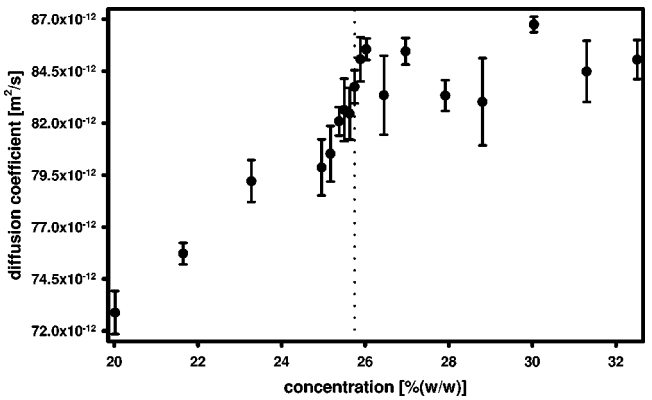

FIG. 10. The diffusion coefficients at 40 °C close to and in the stiff gel region are shown as a function of concentration. The dotted line symbolizes the gel transition.

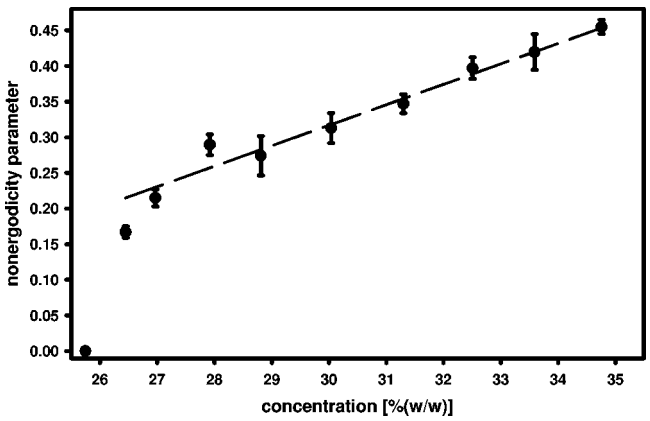

FIG. 11. The nonergodicity parameters are plotted vs concentration. The measurements were performed at 40 °C. (The dashed line is a linear fit to guide the eye.)

low temperatures. This rather broad correlation function has a mean decay time of about 10^{-3} s. The system is a mixture of unimers, micelles, and some larger aggregates, only existing at low temperatures [5].

After entrance into the gel phase [starting at 17.6 °C at 35% (w/w)], the situation changes dramatically: A second (slower) decay appears and the fast decay is shifted to shorter times. The correlation time of the fast mode decreases from 1.82×10^{-5} at 19 °C to 1.07×10^{-5} at 35 °C. The correlation time of the slow mode increases from 2.39×10^{-2} at 19 °C to 9.96×10^{-2} at 35 °C. The relative amplitudes of the fast and slow diffusional modes decrease with temperature at the expense of the increasing nonergodic contribution.

V. DISCUSSION

The binary P94-water system shows a very interesting phase behavior. At low temperatures, water is a good solvent for the triblock copolymer. So most of the polymer chains exist as unimers in solution. Some large aggregates still remain undissolved due to the low solubility of some byproduct in the production process. These aggregates could be

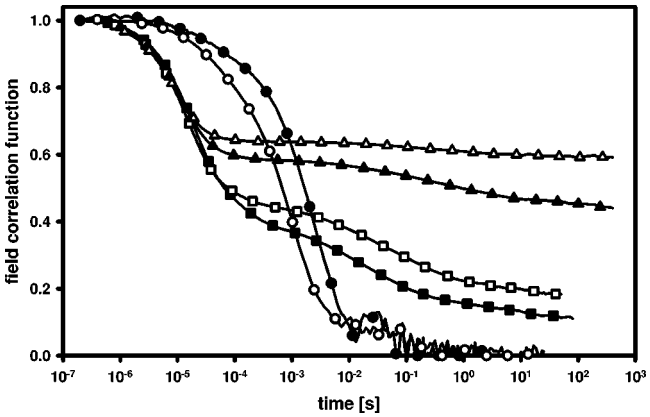

FIG. 12. Field correlation functions at 35% (w/w) and different temperatures are plotted vs time. The curves correspond to the following temperatures: ● 5, ○ 10, ■ 19, □ 23, ▲ 30, and △ 35 °C.

removed at low temperatures by simple filtration with a 200-nm filter. They can be identified as hydrophobic entities as they can also be removed by a solid phase extraction column (ENVI18, Supelco). These cleaning procedures were not necessary for the experiments described in this paper, as by raising the temperature, the polymer becomes amphiphilic that leads to self-assembly into micelles. A few large aggregates also dissolve into the micelles, as can be seen from DLS data from ergodic systems. The DLS shows that the large aggregates disappear when micelles are formed, i.e., at 40 °C. P94 solutions show only one decay in the ergodic concentration regime. The decay constant and the signal strength are same within the statistical accuracy for the untreated or the filtered sample, i.e., the amount of hydrophobic impurities is negligible and does not influence the results in the micellar regime. The core of the micelles formed over a relatively wide temperature regime consists mostly of polypropylene and the shell of polyethylene blocks highly penetrated with water. The phase diagram can be shifted in temperature by varying the absolute block lengths and the amount relative to each other [8,9].

The most interesting feature is the stiff gel region, most probably a cubic phase. The exact determination of the gel structure is hindered by the formation of small microcrystals in the gel. These few crystals have an arbitrary, but fixed orientation (at least in terms of the measurements) and the SAXS data have in most cases a lot of bright spots on top of the diffuse background. For the comparable P85 system, the reflections can be indexed in accordance with a cubic $Pn3m$ structure (scattering peak position ratios $\sqrt{2}$, $\sqrt{3}$, 2, $\sqrt{6}$) and a lattice constant of 14.8 nm, very close to the micellar diameter at a low concentration of 15 nm (unpublished results). The phase boundary into this region appears at about half the concentration one would expect for compact hard spheres. We see from all our data that the volume need of this core-shell micelles is clearly higher than the specific volume of the polymer solubilized. One can imagine that the core consists of a rather compact polypropylene phase (even though less dense than the corresponding bulk phase [5]), where otherwise the shell consists of polyethylene arms reaching into the aqueous solution. SAXS data allow separation of the particle form factor and the structure factor controlled by particle interactions. The micelles have an outer diameter of about 15.5 nm and are close to spherical symmetry—as indicated by the pronounced side maxima in their scattering function. The particle interactions can be represented by a simple hard sphere interaction with an interaction radius of about 7.4 nm or a minimum center-to-center distance of 14.8 nm and a polydispersity of a few percent only. The effective volume fraction determined from the structure factors is more than twice the weight fraction. These results can be understood with a relatively open shell structure of highly hydrated PEO, making this shell relatively stiff. This stiffness is indicated by a hard sphere radius and the diameter of the micelles being practically constant over the wide concentration range measured.

A similar result was obtained from the independent static light scattering data. This technique measures only at very low scattering vectors and it is therefore impossible to get detailed information on the form factor. Under the assumption of a constant form factor, i.e., the higher the concentration the more micelles of the same type are formed, we can divide the scattering intensity by concentration. The resulting curve can be fitted with a theoretical $S(0)$ for a hard sphere Percus-Yevick model with an effective volume fraction of 2.2 times the mass fraction, in perfect agreement with the SAXS results. This factor helps in understanding why the glass transition already occurs below 27% (w/w).

While SAXS and SLS are static methods resulting in information about the mean positional order of the system, we can independently find information about the interaction of the particles from the diffusion dynamics using DLS. As in SLS, we have to assume that the size of the micelles does essentially not change with concentration, which has been established from the SAXS results. In the fluid, ergodic regime we found that the particles behave also dynamically similar to hard spheres, with a hydrodynamic radius $R_H = 8.8$ nm and an effective volume fraction of 2.17 times the mass fraction. These results are in excellent agreement with the static results and one might think that this is an obvious finding, taking into account that the hydrodynamic radius is usually larger due to the bound hydration water which is not seen by the x-rays. However, there exist other systems, such as inverse micelles and water in oil microemulsions, where the static results can also be interpreted as hard sphere interaction, but with strong interpenetration. Such systems show in DLS a diffusion coefficient strongly decreasing with concentration, even though the particles remain globular [24].

It is astonishing to see that the simple linearized approximation [Eq. (9)] for D_{eff}, developed for moderate concentrations holds up to the gel regime. This might be due to the small size of the micelles and due to the specific hydrodynamic interactions with the hydrated polymer shell.

The viscosity data are also in quite good agreement with the scattering data. However, there we cannot get good fits with a simple, linearized model. The model of Mooney [22], which is based on Einstein's viscosity equation but extended to apply to suspensions of finite concentration, can fit the data up to about 22% (w/w). The self-crowding factor is 1.42, if the volume fraction is fixed to 2.1 times the mass fraction, as indicated by the scattering experiments. Mooney found a self-crowding factor of 1.43 for viscosity data from glass spheres. The deviation at the highest weight fraction studied can be due to the finite stiffness of the micelles.

Now we move toward nonergodic stiff gel. From the DLS data, in Fig. 5 we can see that there is a continuous transition of the collective diffusion of the ergodic micellar solution into the fast mode in the nonergodic gel, which does not depend on concentration, while the nonergodicity parameter increases nearly linearly for concentrations above 27% (w/w) corresponding to effective volume fractions higher than 0.58. In addition to this nonergodic term, which appears like a base line in the ensemble averaged correlation function, we also observe a second, slow mode with a relatively small amplitude. Both modes have been proven to be diffusive, according to their q^{-2} dependence. Their amplitude ratio is independent of the scattering angle, i.e., they originate from structures of similar size. But we know that

the fast mode is the collective diffusion of the small micelles, i.e., this term should have no angular dependence. In addition, we could show with additional experiments that both terms have no q dependence. We can understand the fast mode as a ''rattling in the cage'' motion, while the slow mode can be understood as the diffusive motion of small-sized inhomogeneities such as empty positions in the gel.

The frozen state shows a strong increase of intensity toward low scattering vectors. The Guinier approximation, calculated to obtain a rough estimation of the size of the frozen state, shows that the structures are larger than the resolution. With a minimum scattering vector of 0.0084 nm^{-1}, it is only possible to measure structures up to 374 nm in diameter.

The correlation functions for constant concentration but varying temperatures are more difficult to discuss. The phase diagram shows the coexistence of unimers and micelles at low temperatures. We could not reach a region where only unimers exist in aqueous phase, for this would be below 0 °C. We see, therefore, from the beginning at low temperatures a broad decay in the correlation function with an extended tail at high correlation times before the field correlation functions finally go to zero. Some large aggregates or crystallites of hydrophobic material are present in the sample, but they increasingly disappear with temperature in the signal for the micellar system in the diluted micellar solutions. This can be understood as a solubilization of hydrophobic impurities in the micelles.

More and more micelles are formed when the temperature is increased at constant concentration. The advantage of this experimental series is the fact that it can be performed with one sample preparation, so there can be no artifacts introduced by sample preparation and thermal history. In the case of the 35% (w/w) solution, the gel point is reached at 17.6 °C, corresponding to an effective volume fraction of the micelles of about 56% (v/v). Inside the gel the formation of micelles goes on with temperature. This corresponds to an increase of the effective volume fraction of micelles, however, in a not so well defined way. More than that, we have a changing concentration of remaining unimers in the solvent affecting the hydrodynamic interactions on top of the temperature dependence of the diffusion process. In the gel phase the volume fraction of micelles is high enough to start the onset of the formation of cages of micelles to their nearest neighbors. The fast and slow modes have the same origin as in the previous series. The slow mode becomes slower with temperature (concentration) and decreases in relative amplitude due to the increasing packing ratio. The increase of the amplitude ratio of the fast to the slow mode can be interpreted in terms of a decrease in the relative amount of diffusive faults. This goes along with a relative increase of the nonergodic states.

In principle, one could argue that the slow mode might come from some large, but still mobile localized aggregates in the gel, where the huge size gives rise to long correlation times. This idea is, however, in full contradiction with the finding that the slow mode has no angular dependence on amplitude, a feature in common with the fast mode, i.e., both modes must come from entities of comparable sizes. This clearly excludes the possibility of slowly diffusing large structures.

Summarizing we can say that this triblock copolymer system forms interesting phase structures, which can be tuned by variation of temperature and concentration. The transparent phases through the whole phase diagram make the system an ideal candidate for light and x-ray scattering experiments. The structures are small enough to be investigated by small-angle x-ray and neutron scattering. The small size of the objects, together with the relatively low optical contrast, makes the system ideal for light scattering investigation, as the sample is clear in the whole one-phase region. The specialty of this system is also the fact that the size of the objects is much smaller than the q range explored in the DLS and SLS experiments, i.e., there is negligible q dependence on the form and structure factors or, in other words, we measure at $q \approx 0$. This opens new insights into the dynamics of nonergodic systems compared to real hard sphere colloidal systems in the size range of the wavelength of the laser light.

ACKNOWLEDGMENTS

We acknowledge helpful discussions with R. Klein, Konstanz, P. Pusey, Edinburgh, and K. Dawson, Dublin. This work was supported by the Austrian ''Fonds zur Förderung der wissenschaftlichen Forschung'' under Grant No. P12611-CHE.

[1] P. Bahadur and K. Pandya, Langmuir **8**, 2666 (1992).
[2] E.B. Jorgensen, J.H. Jensen, and S. Hvidt, J. Non-Cryst. Solids **172**, 972 (1994).
[3] S. Hvidt, E.B. Jorgensen, W. Brown, and K. Schillen, J. Phys. Chem. **98**, 12320 (1994).
[4] K. Mortensen and J.S. Pedersen, Macromolecules **26**, 805 (1993).
[5] O. Glatter, G. Scherf, K. Schillen, and W. Brown, Macromolecules **27**, 6046 (1994).
[6] M. Malmsten, P. Linse, and K.W. Zhang, Macromolecules **26**, 2905 (1993).
[7] M. Almgren, W. Brown, and S. Hvidt, Colloid Polym. Sci. **273**, 2 (1995).
[8] G. Wanka, H. Hoffmann, and W. Ulbricht, Macromolecules **27**, 4145 (1994).
[9] K. Mortensen and W. Brown, Macromolecules **26**, 4128 (1993).
[10] H. Schnablegger and O. Glatter, Appl. Opt. **30**, 4889 (1991).
[11] P.N. Pusey and W. VanMegen, Physica A **157**, 705 (1989).
[12] A. Bergmann, D. Orthaber, G. Scherf, and O. Glatter, J. Appl. Crystallogr. **33**, 869 (2000).
[13] B. D'Aguanno and R. Klein, in *Light Scattering Principles and Development*, edited by W. Brown (Oxford University Press, Oxford, 1996).
[14] J. Brunner-Popela and O. Glatter, J. Appl. Crystallogr. **30**, 431 (1997).

[15] O. Glatter, Acta Phys. Austriaca **47**, 83 (1977).
[16] O. Glatter, J. Appl. Crystallogr. **10**, 415 (1977).
[17] A. Bergmann, G. Fritz, and O. Glatter, J. Appl. Crystallogr. **33**, 1212 (2000).
[18] D.E. Koppel, J. Chem. Phys. **57**, 4818 (1972).
[19] G. Fritz, G. Scherf, and O. Glatter, J. Phys. Chem. B **104**, 3463 (2000).
[20] D. Lehner, H. Lindner, and O. Glatter, Langmuir **16**, 1689 (2000).
[21] D.J. Kinning and E.L. Thomas, Macromolecules **17**, 1712 (1984).
[22] M.J. Mooney, J. Colloid Sci. **6**, 162 (1951).
[23] H. Lindner and O. Glatter, Part. Part. Syst. Charact. **17**, 89 (2000).
[24] O. Glatter, D. Orthaber, A. Stradner, G. Scherf, M. Fanun, N. Garti, V. Clément, and M.E. Leser, J. Colloid Interface Sci. **241**, 215 (2001).